Case Studies in Thermal Engineering 79 (2026) 107817

Contents lists available at ScienceDirect

Case Studies in Thermal Engineering

journal homepage: www.elsevier.com/locate/csite

Impact of moving arc-shaped segment and optimized splitter on the convective-radiative heat transfer in an inverted T-shaped cavity

Muneer Ismael [a,b], Mohamed Bechir Ben Hamida [c,*], Mehdi Ghalambaz [d,e]

[a] Department of Mechanical Engineering, College of Engineering, University of Basrah, Basra, Iraq
[b] College of Engineering, University of Warith Al-Anbiyaa, Karbala, Iraq
[c] Deanship of Scientific Research, Imam Mohammad Ibn Saud Islamic University (IMSIU), Riyadh, Saudi Arabia
[d] Department of Mathematical Sciences, Saveetha School of Engineering, SIMATS, Chennai, India
[e] Refrigeration and Air Conditioning Technical Engineering Department, College of Technical Engineering, The Islamic University, Najaf, Iraq

GRAPHICAL ABSTRACT

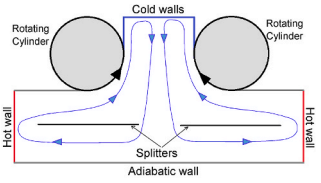

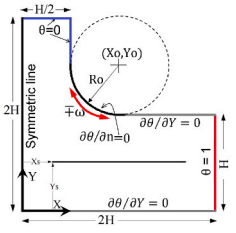

ARTICLE INFO

Keywords:
Convective-radiative

ABSTRACT

The purpose of this study is to maximize the utilization of a heat sink by optimizing the fluid circulating inside an enclosure undergoing convective and radiative heat transfer. Two

* Corresponding author.
E-mail address: MBHamida@imamu.edu.sa (M.B. Ben Hamida).

https://doi.org/10.1016/j.csite.2026.107817
Received 13 December 2025; Received in revised form 31 January 2026; Accepted 8 February 2026
Available online 9 February 2026

Splitter
Rotating cylinder
Moving wall
Optimization
Cavity

mechanisms; moving arc-shaped surface and optimally fluid guiding towards the active walls do the fluid circulation. The two mechanisms of enhancing convective-radiative heat transfer inside an inverted T-shaped enclosure are achieved by rotating a contact cylinder to form an arc-shaped moving surface and inserting an adiabatic thin splitter to guide the fluid towards the heat hot wall. The computations are performed numerically using Galerkin FEM for a symmetric half of the physical domain and for parameters: Reynolds number (Re = 100–500), radiation parameter (Rad = 0–5), horizontal position of the splitter (Xs = 0.05–0.25), and vertical position of the splitter (Ys = 0.05–0.45). The splitter's position is optimally determined using the Nelder-Mead optimization algorithm. The outcomes show that the clockwise movement of the arc-shaped segment guides the fluid to be consistent with the lifted buoyancy force, making it 50% more effective than the counterclockwise direction, which leads to opposite vortices. The splitter provides a 19% gain in convective heat transfer. Its optimum position is given for each Reynolds number, where, with a higher Reynolds number, the splitter should be displaced from the enclosure's centerline and the arc-shaped rotating surface. The radiation parameter plays a similar role to the Reynolds number, proportionally augmenting the overall heat transfer. The study presents a new coupling of two mechanisms, arc-shaped moving wall and a locally optimized divider to circulate the heat transfer fluid in a novel inverted T-shaped cavity.

Nomenclature

AR	absorption coefficient of thermal radiation (m^{-1})	Nu_m	Mean Nusselt number
H	Side wall of the enclosure (m)	Pr	Prandtl number
k	Fluid thermal conductivity ($W.m^{-1}.K^{-1}$)	Ra	Rayleigh number
n	Normal vector (m)	Rad	Radiation parameter
Ro	Radius of the moving ASS (m)	Re	Reynolds number
T_c	Cold temperature (K)	Ri	Richardson number
T_h	Hot temperature (K)	**Greek symbols**	
U	Velocity vector, (u,v) (ms^{-1})	α	Thermal diffusivity (m^2s^{-1})
$\mathbf{U}_t$	Tangential velocity vector (ms^{-1})	θ	Non-dimensional temperature
Xo	Horizontal coordinate of moving ASS (m)	ν	Kinematic viscosity ($m^2.s^{-1}$)
Xs	Horizontal coordinate of the splitter left edge (m)	σ	Stephan-Boltzmann constant ($W.m^{-2}K^{-4}$)
Yo	Vertical coordinate of moving ASS (m)	ω	Angular speed (rad/s)
Ys	Vertical coordinate of the splitter left edge (m)	**Abbreviations**	
Dimensionless parameters		ASS	Arc-shaped segment
Gr	Grashof number	TBL	Thermal boundary layer

1. Introduction

As an ever developing of industrial applications, heat removal from hot surfaces is crucial across divers industries and applications, primarily to ensure operational efficiency and prevent equipment degradation. The ability to effectively dissipate heat is fundamental in fields ranging from nuclear energy [1] to save electronics from damage [2]. When the hot surfaces are housed in an enclosed spaces, then proper circulation of the fluid inside enclosures enhances the efficient energy exchange between the cooled heat sink and the source of heat. Utilizing the no-slip condition, driven boundaries ads kinetic energy to the contacting fluid based on the friction between the solid moving boundaries and the contacting fluid. This mechanism, which triggers the natural convection to the forced convection, is widely investigated in enclosed domains to transport the thermal energy from its source to a sink zone [3–5], with the inclusion of; the magnetic field effect [6], the nanoparticles [7], and to convey the species from high concentrated walls to the low one [8–10]. Given its importance in the industry, studies continue to develop this topic. Abedallh et al. [11] did numerical and experimental comparisons for a cavity with several aspect ratios and a restricting lid. They drove the lid in sinusoidal motion with various periods. By assuming negligible weight for the white smoke particles, streamlines were followed by generating white smoke, which was driven by buoyant rising air. Their outcomes showed a rise in the *Nu* number with a rise in the reciprocating lid's period. Saleem et al. [12] suggested an alternative benefit of the moving wall in expediting the melting process of a phase change material (PCM). They assumed a sinusoidal reciprocated hot base of a cavity filled with a PCM and enhanced by carbon nanotubes (CNTs), and they followed the variation and speed of the melting front toward the cold upper wall. They revealed that the amplitude of the sinusoidal motion noticeably affected the speed of paraffin melting. When the amplitude was boosted from 0.1 m/s to 0.3 m/s, the amount of molten liquid rose by 17% for uniform motion and 21% for sinusoidal motion. Alomari et al. [13] proposed a combined lid that provides an evenly divided lid, with each part moving opposite to the other. Such a split-moving lid was kept cold [13] and adiabatic [14]. In both studies, the base was heated partially [13] or totally [15], and the speed of the two opposite parts of the lid contributed notably to raising the Nusselt number. Unless the applied magnetic field was triggered, such lid motion generated symmetric temperature distribution and streamlines within the curvilinear-shaped enclosure they studied. Chamkha and Ismael [16] and Ismael and Chamkha [17] addressed the importance of the moving direction of a trapezoidal enclosure's slanted wall. For predominant forced convection, the wall movement should be upward, aligning with the buoyancy force. Conversely, for predominant free convection, wall movement opposite to the buoyancy force is beneficial. Because these two studies conducted computations using a regular finite

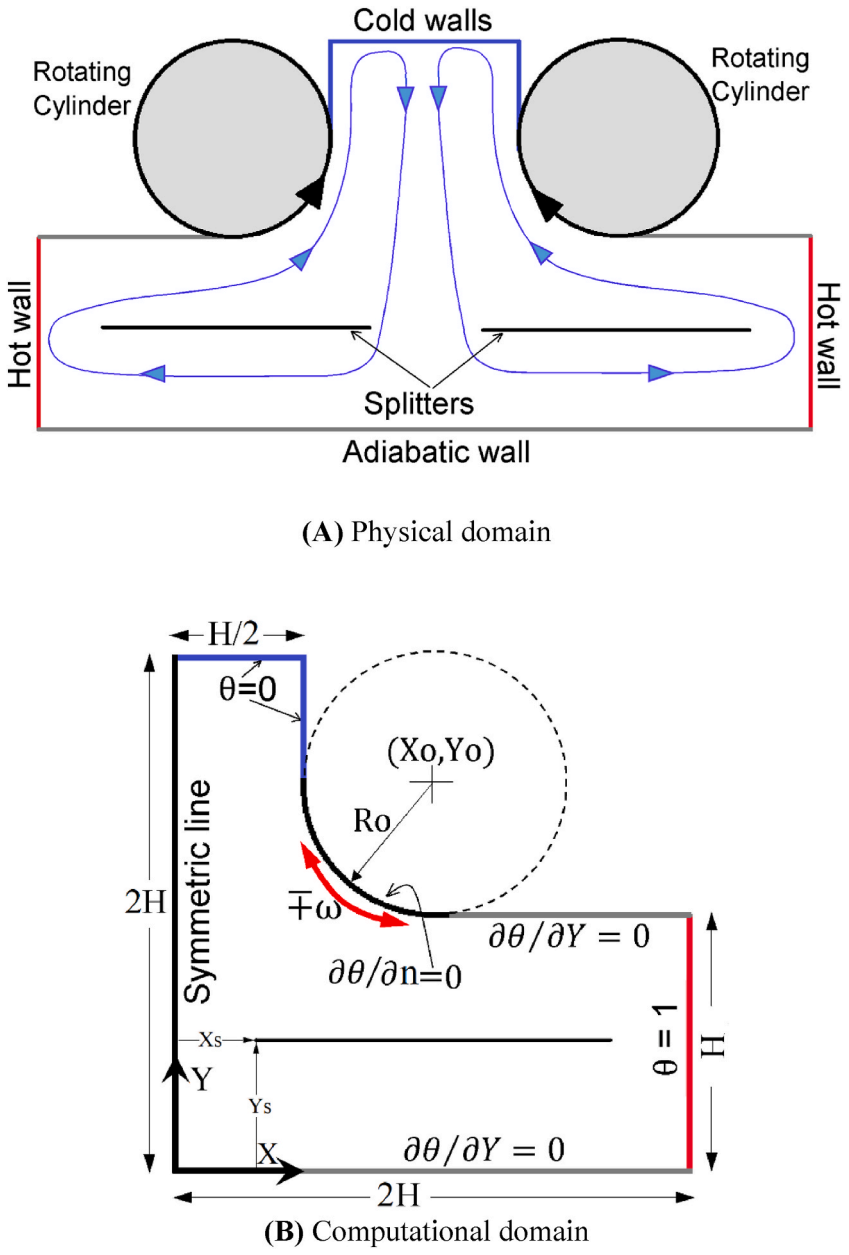

Fig. 1. Physical (A) and computational (B) domains of the problem.

difference scheme, they showed that care should be taken in selecting the sidewalls' inclined angle to align grid points with the physical sidewall.

Some scholars delved into the complexity of numerical solutions for double-sided moving wall problems. Some studies reported several possible steady solutions in cases of significant inertial forces [18], where they measured distinct solutions based on the variation of point and/or line streamline symmetry. Blohm and Kuhlmann [15] conducted experimental flow visualization to endorse the results of [18] by realizing the moving sidewalls with two tightly closed, rotating drums with large radii. However, they approximated the curvature of the contacting drums and compared the visualized flow patterns with the plane moving sides' case. The development of numerical manipulations has solved the technical problems resulting from the discretization of irregular boundaries. For instance, Ismael [19] solved the problem of an arc-shaped moving wall by using an adaptive finite difference method. By adapting the mesh nodes, the curvature of the moving arc is covered by sufficient mesh nodes. As such, the study was unique in exploring the impacts of the direction and the curving of the moving wall on mixed convection. This adaptive numerical method was applied further to study the transport of heat and mass concentration within a partially-porous enclosure [20]. Thereafter, studies of arc-shaped moving walls were triggered by considering a tightly contacting rotating cylinder, and delved into several aspects of heat transfer

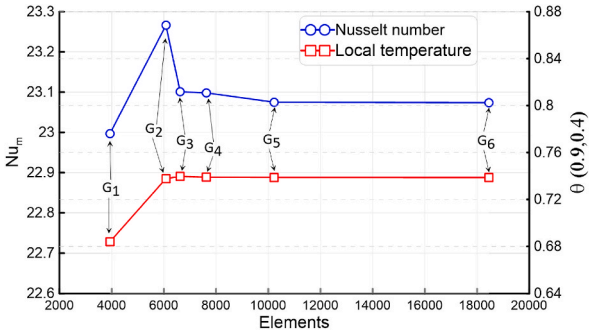

Fig. 2. Mesh dependency test against the mean Nusselt number and the dimensionless temperature at a position X = 0.9 and Y = 0.4.

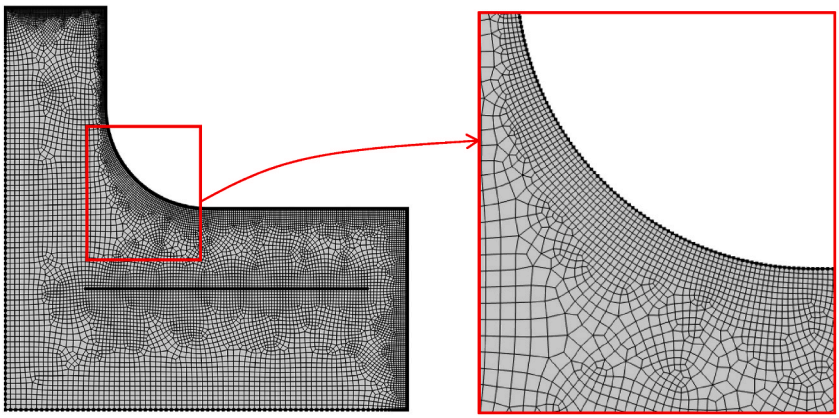

Fig. 3. The adopted quadrilateral mesh of the numerical solution.

Table 1
Ranges of the investigated parameters.

Description	Parameter	Min. value	Max. value
Radiation parameter	Rad	0	5
Horizontal coordinate of the left splitter edge	Xs*H/2	0.05	0.25
Vertical coordinate of the left splitter edge	Ys*H/2	0.05	0.45
Reynolds number	Re	100	500

Table 2
Computational mean Nusselt number on a top hot wall: a benchmark of Iwatsu et al. [3] and Sharif [4], top moving wall.

Re	*Gr*								
	10^2			10^4			10^6		
	Iwatsu et al.	Sharif	Present	Iwatsu et al.	Sharif	Present	Iwatsu et al.	Sharif	Present
100	1.94	-	2.039	1.34	-	1.400	1.02	-	1.021
400	3.84	4.05	4.090	3.62	3.82	3.853	1.22	1.17	1.182
1000	6.33	6.55	6.616	6.29	6.50	6.568	1.77	1.81	1.785

in different fluids [21,22].

As a passive tool for assisting in heat transport, adiabatic baffles are equipped in enclosures to help control fluid circulation. With lid-driven problems, the role of the baffles emerges due to strong fluid dynamics. Ma et al. [23] showed that a vertically dangled baffle compresses the vortices formed by driving the lid of a U-shaped cavity. They proposed a limited length for the baffle (not more than 0.4 of the cavity wall), where a prolonged baffle adversely affects fluid circulation. Azizul et al. [24] designed three ladder-shaped baffles inside a driven wall enclosure with wavy walls. They observed that the baffles closer to the moving wall were more active in constricting the circulation. Essfe et al. [25] investigated three alternative wall-mounted baffles. These baffles were maintained at an isothermal hot temperature. Recommendations included shortening baffle length and widening the distance between them. Ji et al.

Table 3
Computational mean Nusselt number on the bottom hot wall: a benchmark of Yapici and Obut [5], top moving wall.

Re	*Gr*					
	10^2		10^4		10^5	
	Yapici and Obut [5]	Present	Yapici and Obut [5]	Present	Yapici and Obut [5]	Present
100	4.2921	4.278	4.1454	4.1540	6.5329	6.588
400	-		8.5157	8.430	-	
1000	-		14.0077	14.053	-	

[26] pioneered the design of multiple wall-mounted baffles to enhance free convection during the melting of the PCM. They demonstrated that controlling the spacing between baffles creates grooves that blend upward hot and downward cold liquids, thereby decreasing temperature variation. They also demonstrated the baffles' ability to alter the behavior of molten fluid circulation. Lorenzini et al. [27] reported that a thick, base-mounted hot fin significantly enhanced the Nusselt number in a driven-lid cavity. They explored several aspect ratios of the rectangular fin. Moayedi et al. [28] explored four different shapes of base-protruded hot fins. They found that when the fin has a 90-degree bend aligned with the rout of the moving upper lid, heat transfer is maximized. Ali et al. [29] considered a whirling plate with upper moving lid cavity and reported the importance of the length and the whirl speed on the enhancement of heat transfer.

When an element rotates within the heat exchange domain, the mixing process becomes active and produces efficient heat transfer. The rotating internal element can be a circular cylinder [30] or a roughened cylinder [31]. Ikram et al. [32,33] formulated a problem of a rotating baffle acting as a flow-stirring modulator inside a hexagonal cavity. They designed a multi-blade modulator but reported a marginal role for the number of blades in the modulator [34].

Consequently, the survey indicates that mixed convection in rectangular enclosed spaces can be significantly influenced by moving the lid or other sidewalls. It also suggests that moving arc-shaped walls have not been extensively investigated. Baffles within cavities are commonly designed as tabulators or mixers. However, their use as splitters is rarely studied. To address this gap, a baffle is inserted into a specific cavity geometry. The baffle's role is to split and guide the flow to the target hot surface. The splitter's optimal location will be determined using a numerical optimization technique based on an objective function.

Therefore, such a cavity, which drives convection by a shear action imposed by moving arc-shaped walls, facilitates fluid movement between a limited heat sink and two hot surfaces, specifically, a T-inverted cavity. Heat exchange in such a geometry is crucial in preventing equipment degradation in nuclear reactors and protecting electronics from damage.

2. Problem statement

The main aim of the problem under consideration is removing thermal energy from two hot surfaces forming the lower sides of a T-inverted shape cavity by sinking heat to cold walls forming the upper part of the cavity (Fig. 1 (A)). Two rotating drums are tightly contact the curvature zone of the cavity to make one fourth of drum to be an arc-shaped moving surface that induces the fluid motion inside the cavity based on the no-slip boundary condition. Two very thin plates are placed inside, acting as splitter, to prevent the fluid pre-circulation before approaching the hot walls, i.e., to guide the fluid closer to the hot target. By assuming anti-rotating drums and identical splitters, the symmetry help in transforming the physical domain (Fig. 1 (A)) to computational domain (Fig. 1 (B)). The circulation fluid is water at 20 °C (Pr = 6.067), incompressible and Newtonian. The flow is limited to laminar flow and the heat dissipation is safely neglected, while the radiation heat transfer is taken into account. Constant thermophysiacl properties are assumed and the body force represented by the density variation are formed by buoyancy force term in the momentum equation. Geometrically (Fig. 1 (A)), the length of the hot (θ = 1) wall is H while the horizontal lower wall and the symmetric line are 2H long. At the upper cold part (θ = 0) of the cavity, the horizontal and vertical walls are H/2 long. The drum rotates by ∓ω with a radius of Ro = H/2 and centered at Xo = H and Yo = 3 H/2. The splitter length is fixed at 1.4 H and its position is measured by its left edge (Xs, Ys). To normalize the dimensional governing equations to non-dimensional set, the following ratios are arranged to be; Prandtl number $Pr = \nu/\alpha$, Rayleigh number $Ra = g\beta\Delta TH^3/\nu\alpha$, Reynolds number $Re = \omega R_o H/\nu$, Grashof number $Gr = Ra/Pr$, $Ri = Gr/Re^2$

$$(X, Y) = \frac{1}{H}(x, y), (U, V) = \frac{H}{\alpha}(u, v), \theta = \frac{T - T_c}{\Delta T}, \Delta T = T_h - T_c \tag{1}$$

- Mass conservation,

$$\frac{\partial U}{\partial X} + \frac{\partial V}{\partial Y} = 0 \tag{2}$$

- Momentum conservation in X and Y coordinates,

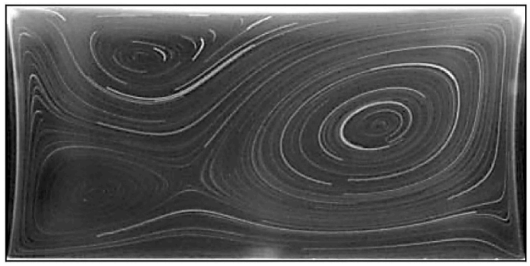

Blohm and Kuhlmann [18]

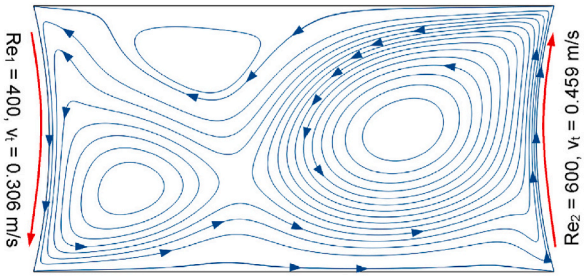

Present result

(A) $Re_1 = 400$, $Re_2 = 600$

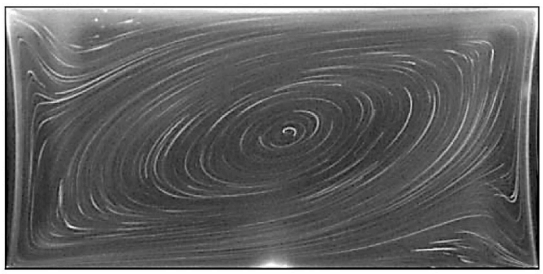

Blohm and Kuhlmann [18]

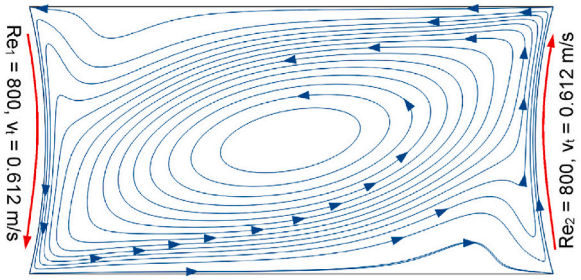

Present result

(B) $Re_1 = Re_2 = 800$

Fig. 4. Validating the current solution with Experimental visualization of the streamlines of Blohm and Kuhlmann [15] for oppositely driven sidewalls with non-equal (A) and equal velocities (B) velocity.

$$\left(U\frac{\partial U}{\partial X}+V\frac{\partial U}{\partial Y}\right)=-\frac{\partial P}{\partial X}+\frac{1}{Re}\left(\frac{\partial^2 U}{\partial X^2}+\frac{\partial^2 U}{\partial Y^2}\right) \tag{3}$$

$$\left(U\frac{\partial V}{\partial X}+V\frac{\partial V}{\partial Y}\right)=-\frac{\partial P}{\partial Y}+\frac{1}{Re}\left(\frac{\partial^2 V}{\partial X^2}+\frac{\partial^2 V}{\partial Y^2}\right)+\frac{Gr}{Re^2}\theta \tag{4}$$

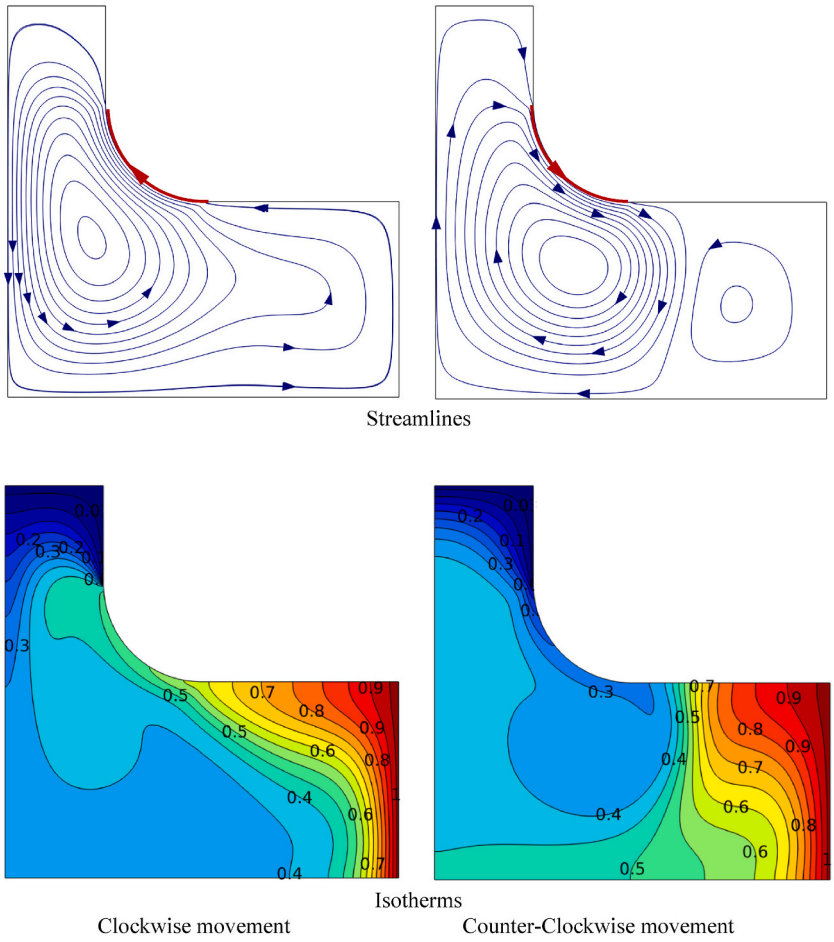

Fig. 5. Influence of rotation direction on the flow circulation and temperature distribution for Re = 200, Rad = 2, clear cavity (no splitter).

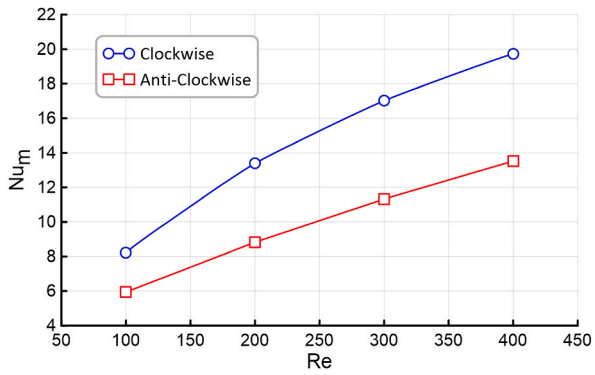

Fig. 6. Mean Nusselt number for clockwise and anti-clockwise rotations.

- Thermal energy conservation [35],

$$U\frac{\partial\theta}{\partial X}+V\frac{\partial\theta}{\partial Y}=\frac{1}{Re\,Pr}\left(1+\frac{4}{3}Rad\right)\left(\frac{\partial^2\theta}{\partial X^2}+\frac{\partial^2\theta}{\partial Y^2}\right) \tag{5}$$

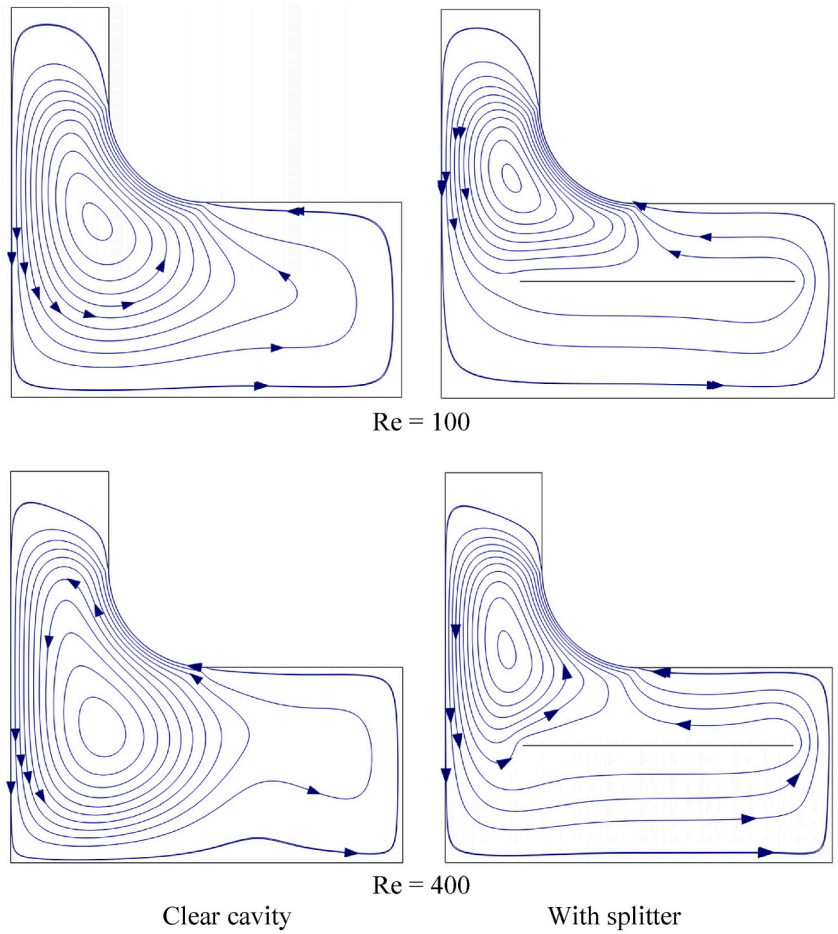

Fig. 7. Influenced streamlines by the role of splitter for Re = 100 and 400, clockwise rotation, Rad = 1, Ys = 3, Xs = 0.2.

where Rad is the radiation parameter defined as [35,36], $Rad = \frac{4\sigma T_c^3}{k\,AR}$, in which the symbol σ implies to the constant of Stephan-Boltzmann, and AR represents the absorption coefficient, quantifying how strongly a material absorbs thermal radiation.

The boundary conditions:

- The top perpendicular segments, representing the heat sink: θ = 0, U = V = 0
- The lower hot vertical surface, representing the heat source: θ = 1, U = V = 0
- The symmetric line, to save the numerical efforts: $\frac{\partial\theta}{\partial X} = \frac{\partial V}{\partial X} = \frac{\partial U}{\partial X} = 0$
- The arc-shaped segment (ASS), resulting from the drum's rotation [19]: $\frac{\partial\theta}{\partial n} = 0$, $\boldsymbol{U} = \boldsymbol{U}_t = \frac{1}{Ro}\sqrt{(Y - Yo)^2 + (Xo - X)^2}$

The velocity vector $\boldsymbol{U} = (U, V) = \{\omega(Y - Y_o), \omega(Xo - X)\}$, $\mathbf{U_t}$ is the tangential velocity and Ro is the drum radius [19].

For the sake of overall heat transfer quantifying, the mean Nusselt number is implemented [36]:

$$Nu_m = \int_0^1 \left(1 + \frac{4}{3}Rad\right)\frac{\partial\theta}{\partial X}\,dY \tag{6}$$

3. Discretizing and solving the computational domain

Discretization is the pivotal point of the numerical solution, which is adopted to solve the suggested problem. Because of the complexity of the geometry under study, the computational domain (Fig. 1 (B)) is discretized by unstructured quadrilateral mesh based on the Galerkin finite element approach. The velocities U and V and the temperature (θ) are expanded based on the basis function $\left[\Phi_i^k\right]_I^M$ for implementing approximation solutions for the velocity, temperature and pressure distributions [37]:

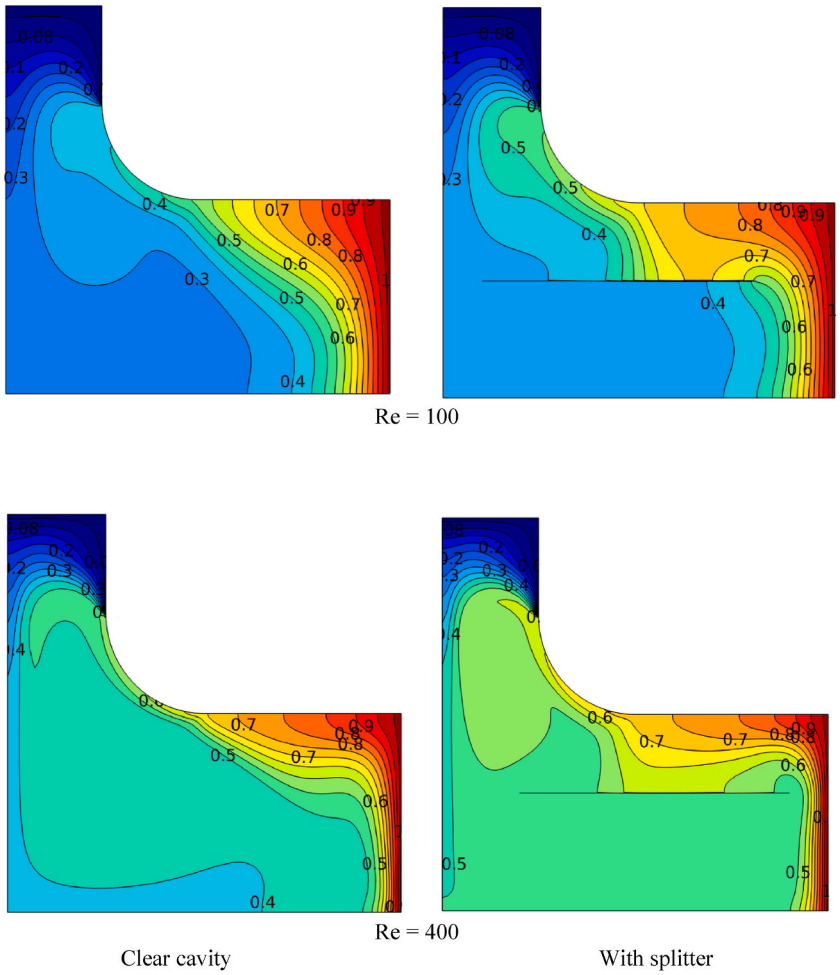

Fig. 8. Influenced isotherms by the role of splitter for Re = 100 and 400, clockwise rotation, Rad = 1, Ys = 3, Xs = 0.2.

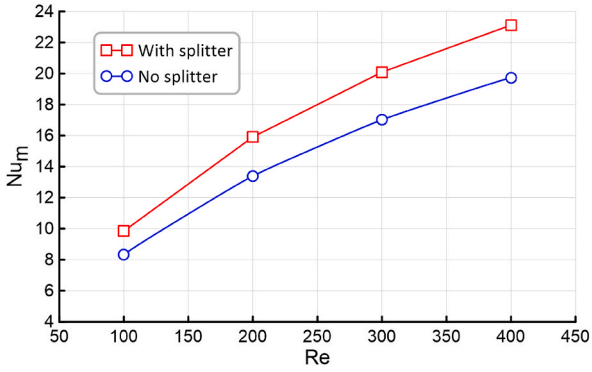

Fig. 9. Mean Nusselt number with and without splitter, Rad = 2, Ys = 3, Xs = 0.2.

$$U, V \approx \sum_{I}^{M} (U, V)_I \Phi_I(X, Y), P \approx \sum_{I}^{M} \mathrm{P}_I \Phi_I(X, Y), \theta \approx \sum_{I}^{M} \theta_I \Phi_I(X, Y) \tag{7}$$

The subscript I and the superscript M refer to the node index and number of nodes, respectively.

Newton-Raphson iteration scheme is invoked to solve the nonlinear residual equations that are obtained from the Galerkin weighted residual finite-element method. The dependent variables are deemed satisfactory when their iterative refinement process

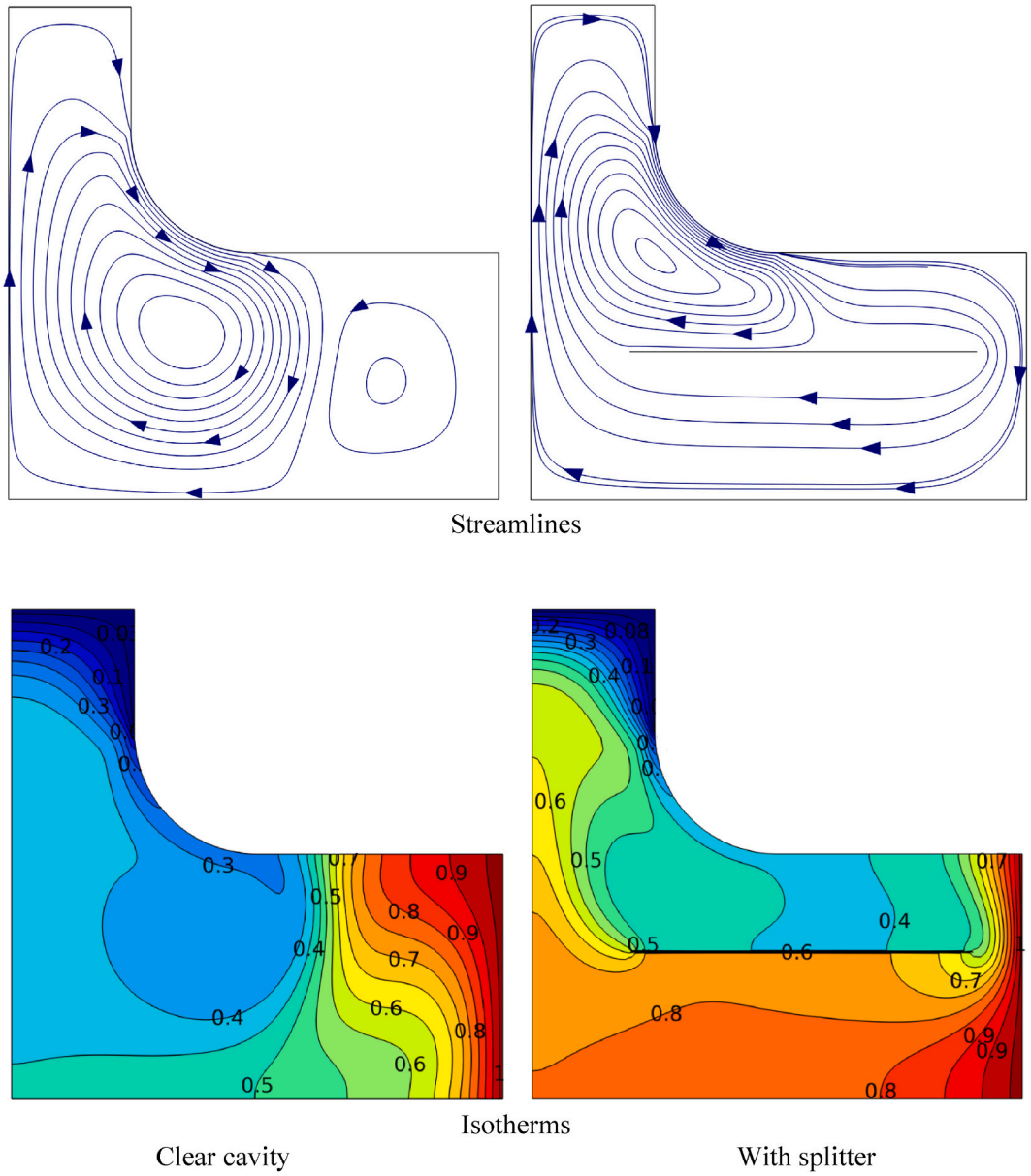

Fig. 10. Influenced streamlines and isotherms by the role of splitter for Re = 200, Counter clockwise rotation, Re = 200, Rad = 2, Ys = 3, Xs = 0.2.

reaches a state of convergence, specifically when the percentage change between successive iterations $\left(\Gamma^{i+1}-\Gamma^{i}\right)/\Gamma^{i+1}$ of either θ, U, V or P is less than or equal to 10^{-5}. The velocity and temperature fields were discretized using a first-order scheme. The pressure gradient was handled with the Penalty method. The mesh nearby the rotating segment and around the splitter are refined to catch the steep changes of the velocity there accurately. To ensure the numerical solution's safety from its dependence on domain discretization size and the absence or spread of singularities, we repeated a specific case's solution for several grids. We then monitored the local temperature at point (0.9, 0.4) and the average Nusselt number, as shown in Fig. 2. This figure indicates the numerical solution's stability after the G_3 grid with 6624 elements, allowing the adoption of any subsequent grid. We adopted G_5 10,230 elements due to the balanced accuracy of results and processor time. The mesh nearby the moving wall, isotheral walls and the splitter are refined as shown in Fig. 3.

Once numerical convergence is guaranteed, a suitable algorithm can be applied to find optimal circumstances to fulfill an objective function. For this sake, we implemented a widely used simple algorithm, namely, the Nelder-Mead method [38]. This method also known as the downhill simplex method, it is a widely used numerical technique for finding a local maximal or minimal of objective function(s) in a multidimensional space. It is a direct search method, meaning it relies on function comparisons rather than derivatives, making it particularly suitable for nonlinear optimization problems where derivatives may be unknown or difficult to compute. Its

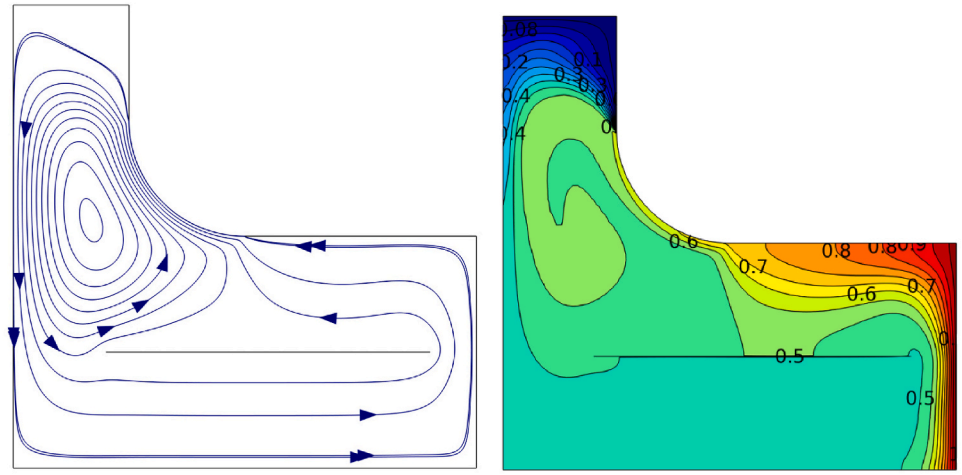

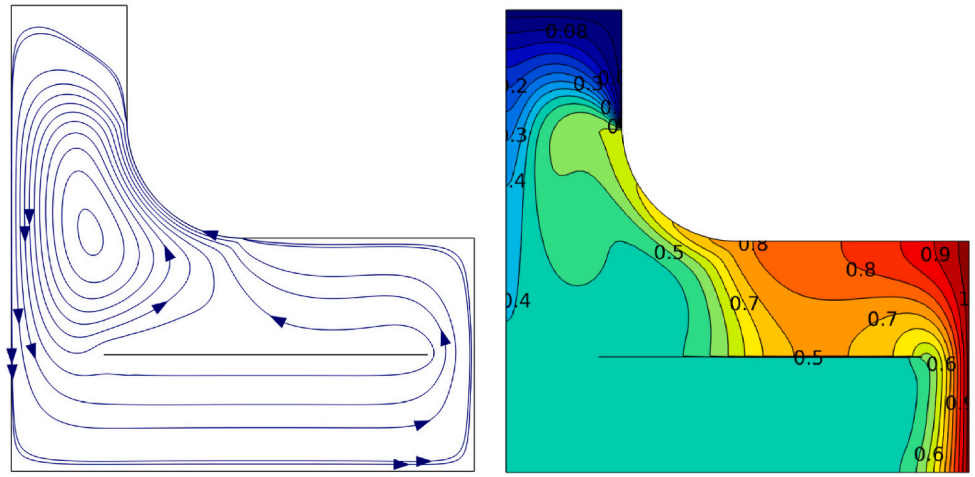

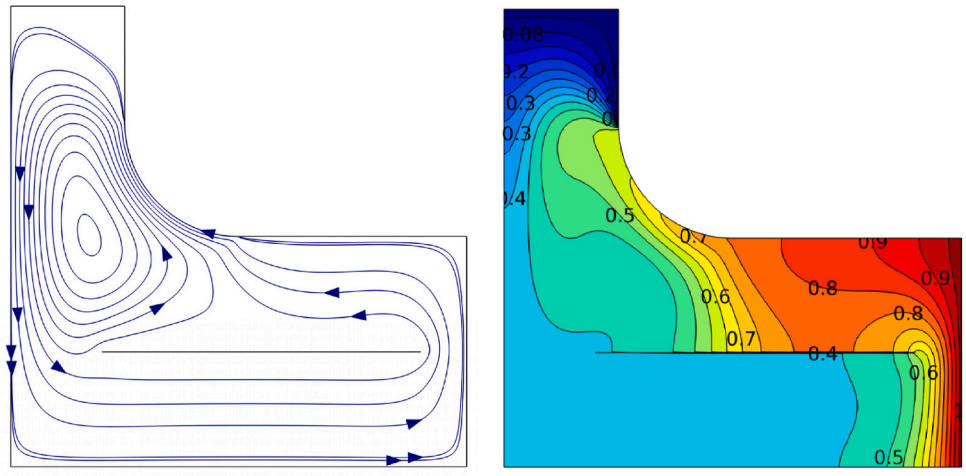

Fig. 11. Impact of the radiation parameter on the isotherms and the streamlines for Re = 300, Ys = 0.25, Xs = 0.2.

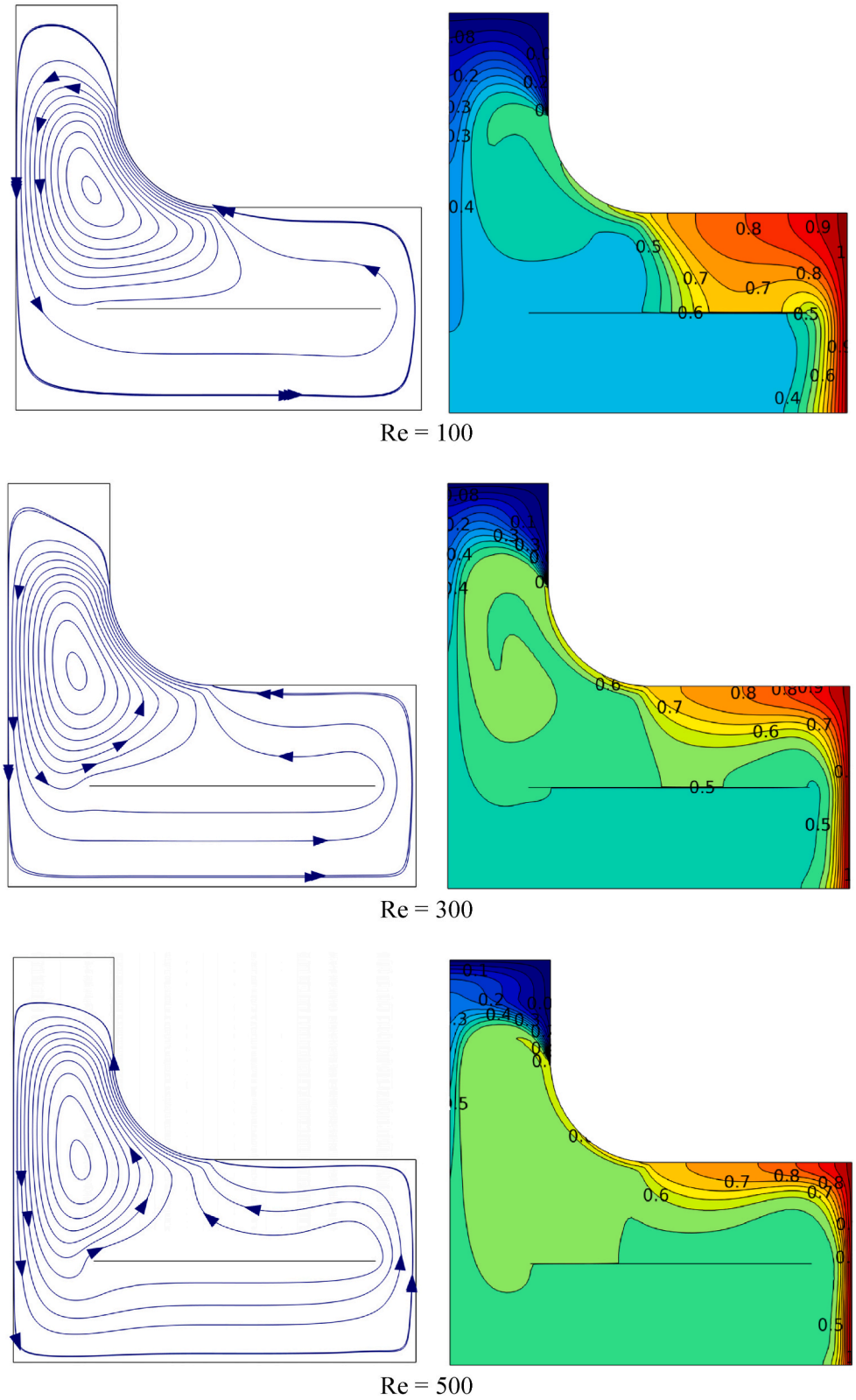

Fig. 12. Impact of the Re number on the isotherms and the streamlines for Rad = 0, Ys = 0.25 and Xs = 0.2.

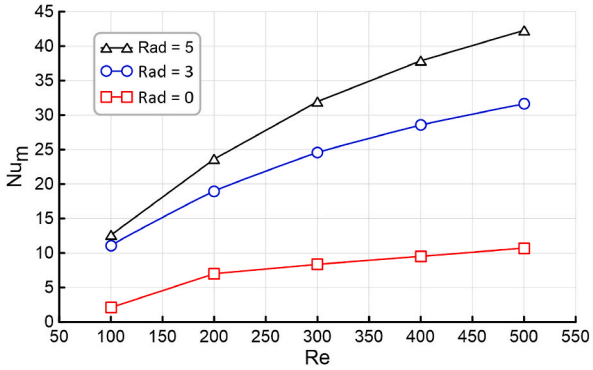

Fig. 13. Mean Nusselt number with Re for different Radiation parameters, Ys = 0.25, Xs = 0.2.

popularity stems from its relative simplicity to understand and implement, and its effectiveness in various fields including statistical problems like parameter estimation. The method often provides significant improvements in function value within the first few iterations and can quickly produce satisfactory results.

4. Results and discussion

Focusing the investigation on the role of the moving arc-shaped segment ASS, guiding the streamlines with the splitter, and taking radiation into consideration, we kept the Prandtl number for water at 20 °C (Pr = 6.067) and the Richardson number in a comparable range (Ri = 1.0). The ranges of the explored parameters are given in Table 1. The results are not compiled until the numerical solution is verified.

4.1. Validating the numerical solution

To confirm the validity of the present numerical solution, a series of benchmark problems are re-solved using the present numerical code. The Nusselt number averaged on a hot moving top lid of air-filled cavity is tabulated in Table 2 compared with Iwatsu et al. [3] and Sharif [4]. Alternatively, when the heating is assigned for the base of water-filled cavity while the top moving lid is kept cold, the results of this comparison with Yapici and Obut [5] is given in Table 3. Although the present results differ slightly from some of those of Iwatsu et al. [3], the most results show good agreements with the other benchmarks.

To delve with experimental validation, the present computations are adopted to solve the experimental hydrodynamics of a silicon oil (Bayar Baysilone) filling a rectangular enclosure with oppositely moving sidewalls. These moving sidewalls are made by contacting the enclosure with two horizontally rotating drums of radii 0.087 m and 0.088 m. For this sake, the present simulations are designed to solve 2D cavity with oppositely moving arc-shaped sidewalls. Two circumstances are solved, equal tangential wall speeds (0.612 m/s) and different tangential wall speeds (0.306 m/s and 0.459 m/s). The results of maps of the streamlines shown in Fig. 4 are consistent with the photos of Blohm and Kuhlamnn [15] taken by hot film probe. The numerical solution implemented in this paper can, therefore, be relied upon.

4.2. The influence of the rotation direction

Since the heat source is located underneath the rotating arc-shaped segment (ASS), then the direction of the rotation may affect the transport of energy via different mechanisms. To demonstrate this sense, clockwise and anti-clockwise rotations are studied for Re = 200 and Radiation parameter of Rad = 2. The maps of the streamlines shown in Fig. 5 present perceptible difference between the paths of the streamlines for each direction. For clockwise rotation, the elevated fluid from the hot zone, due to the buoyant force, engages with the fluid driven by the shear effect of the moving ASS. These two mechanisms combine in raising the fluid towards the cold region at the top of the cavity, where the thermal energy is rejected, then, the fluid falls down to close the circulation loop and forms the main vortex occupying the cavity. Alternatively, for counter-clockwise rotation, counter-rotating vortices form due to the shear effect. This drives the cold fluid towards the hot zone, where it meets the buoyancy-elevated fluid. Along the line of meeting these vortices, the isothermal lines are sharply divided and looks resisted by the driven down fluid. On the other hand, the isothermal lines of the clockwise rotation demonstrate the driven hot fluid continuously towards the cold zone. Hence, the aiding and opposing flows created by clockwise and counter-clockwise rotation, respectively, explain the superiority of the Nusselt number for clockwise rotation over counter-clockwise rotation as given in Fig. 6, where, for example, at Re = 300, the superiority of Nu_m of the clockwise rotation is about 50%.

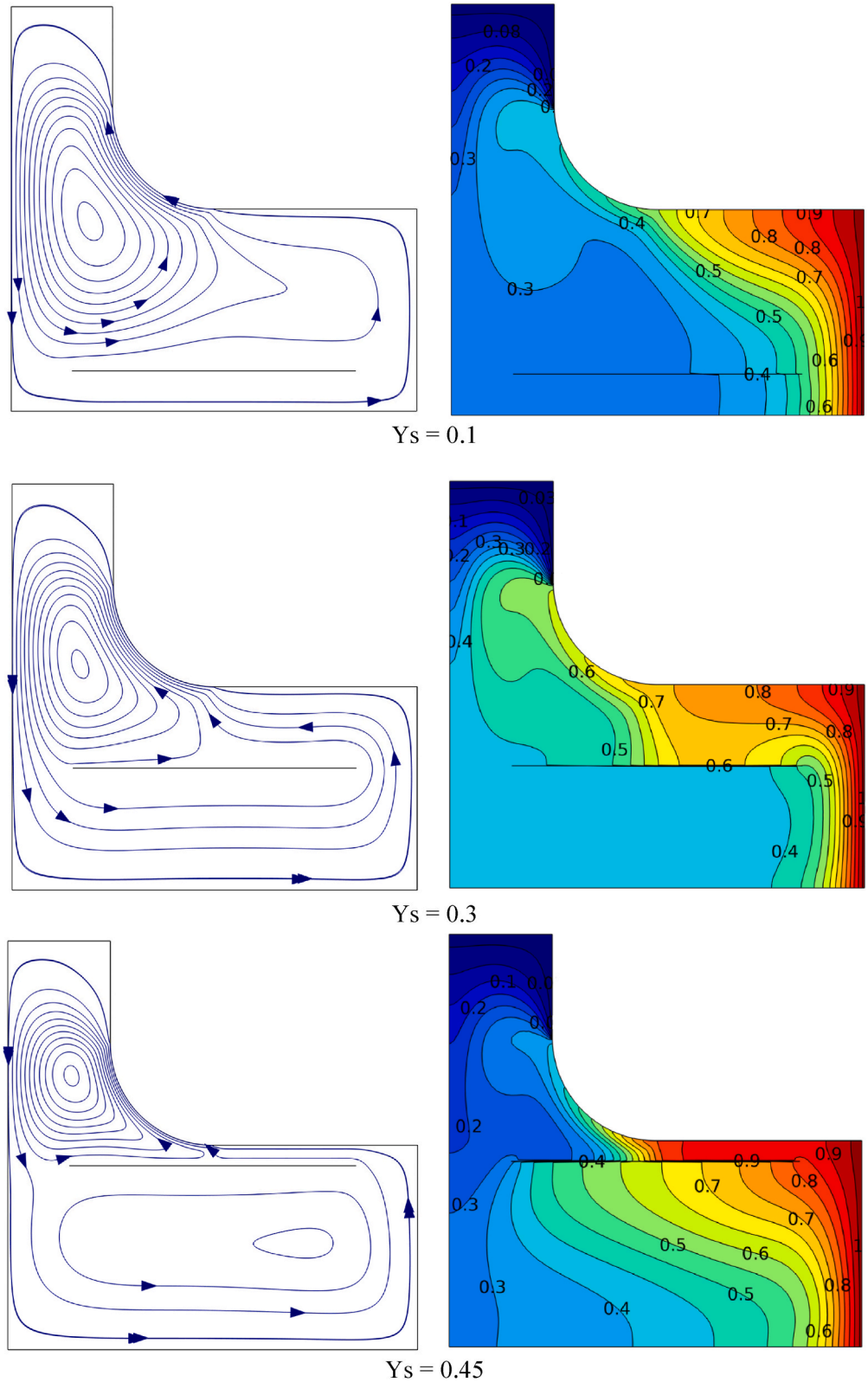

Fig. 14. Impact of the splitter vertical position on the isotherms and the streamlines for Re = 200, Rad = 2, Xs = 0.15.

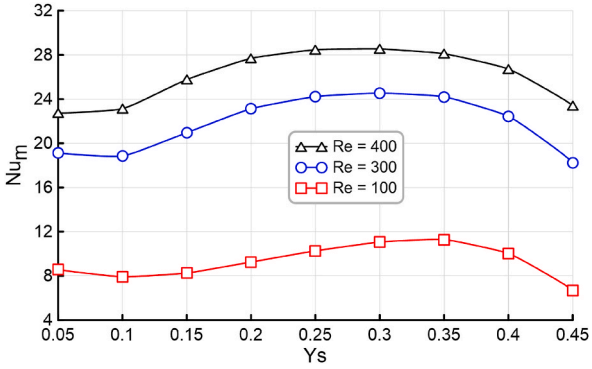

Fig. 15. Mean Nusselt number with the splitter vertical position Ys and different Re numbers.

4.3. The role of the splitter

It is noted from the streamlines of Fig. 5 that the fluid circulation concentrates close to the ASS. To convey the robust energy of this circulated fluid towards the hot zone, it is designed to insert a splitter sheet that can split the strong vortex and guides the fluid towards the hot zone. Fig. 7 demonstrates the role of the splitter on the streamlines for clockwise rotation at Re = 100 and 400. The figure delineates as efficient role of the splitter in shrinking the strong vortex and guiding some fluid towards the hot wall. By setting the splitter as adiabatic sheet, it acts not only as guiding tool, but also separates the elevated fluid carrying higher thermal energy from mixing with the underneath cold fluid, which provides a continuously cold stream when hit the hot wall as can be clearly presented from the temperature distribution depicted in Fig. 8. The virtue of the splitter is evidence by the mean Nusselt number plotted in Fig. 9, which reveals the improvement in the convection heat transfer. Namely, for Re = 200 and 300, the splitter elevates the Nu_m by 19% and 18%, respectively.

For counterclockwise rotation, the role of the splitter is also investigated as shown in Fig. 10. The figure explains a good tool in merging the counter rotating vortices and conveying the cold fluid towards the hot wall. Accordingly, the violently affected thermal boundary layer (TBL) leads to an augmentation in the Nu_m for about 50% and 68% for Re's of 100 and 200, respectively. However, in this case, the driven-down fluid violently impinges the upper face of the splitter and directly faces the buoyancy lifted fluid. This triggers a high perturbation leading to unstable solution, which requires special efforts to overcome the stability of the numerical solution. For this reason, we focuses on the splitter role in clockwise rotation and deferred the counterclockwise to be treated in rather numerical models for future works.

4.4. Influence of the radiation parameter and the Reynolds number

The influence of the radiation parameter (Rad) shows marginal action on the behaviors of the streamlines and the temperature distribution. Nevertheless, the temperature contours explains the settling of the cold fluid underneath the splitter for higher Rad values as shown with Rad = 5 in Fig. 11. This is the indication to the stimulation role of the radiation to the overall heat transfer inside the cavity. Rather, the Reynolds number which is based on the rotational speed of the ASS, reveals the inertial force's role in boosting fluid circulation, thereby robustly transporting the cold fluid towards the hot wall and thinning the TBL, which is evident with Re = 500 in Fig. 12. The values of the mean Nusselt number with Rad and Re are displayed by Fig. 13, showing that the rise of Nu_m with Re is rapid for higher radiation parameter, where by leveraging Re from 200 to 500, the rise in Nu_m are 53%, 67% and 79% for Rad = 0, 3 and 5, respectively. Compared with Rad = 0, the Nu_m of Rad = 3 and 5 at Re = 300 increases by 197% and 282%, respectively.

4.5. The splitter position

Since the splitter role concern with streamlines of the circulated fluid, then it is wise to scrutinize its position, which is measured by its vertical distance from the base, Ys, and the distance of its left edge from the symmetric line of the computational domain, Xs. The vertical distance is varied from Ys = 0.1 (closest to the cavity base) to Ys = 0.45 (closet to the rotating ASS). The lowest distance Ys = 0.1 exhibits small role in driving the fluid as it far away from the core of the vortex, thereby, the TBL undergoes marginal change as can be observed by Fig. 14. On the other hand, lifting the splitter closer to the rotating ASS leads to trap the vortex within the neck (upper part of the cavity). Hence, weak circulation covers a substantial zone of the cavity, which in turn thickens the TBL as can be seen when Ys is set at 0.45. Therefore, it is sought that there is a suitable position between the bonds of Ys. Fig. 15 discovers this suggestion, where there is a maximum Nu_m within Ys ≈ 0.3 – 0.35, while the worst Nu_m is fond at Ys = 0.45. The inspected horizontal position Xs (0.1 – 0.25) is shown in Fig. 16 for Ys = 0.2 and Re = 200. As the splitter is close to the symmetric line, then it permits to little fluid to pass underneath, while when it is shifted towards the hot wall, its right edge restrict the elevated buoyancy fluid as can be noticed with Xs = 0.25 where two distinct TBL's appear. Thus, the Nu_m drops notably with Xs = 0.25 as depicted in Fig. 17. Similar to the vertical distance of the splitter Ys, the horizontal distance Xs does, where for Re > 100, the value of Xs = 0.2 exhibits most favorable position.

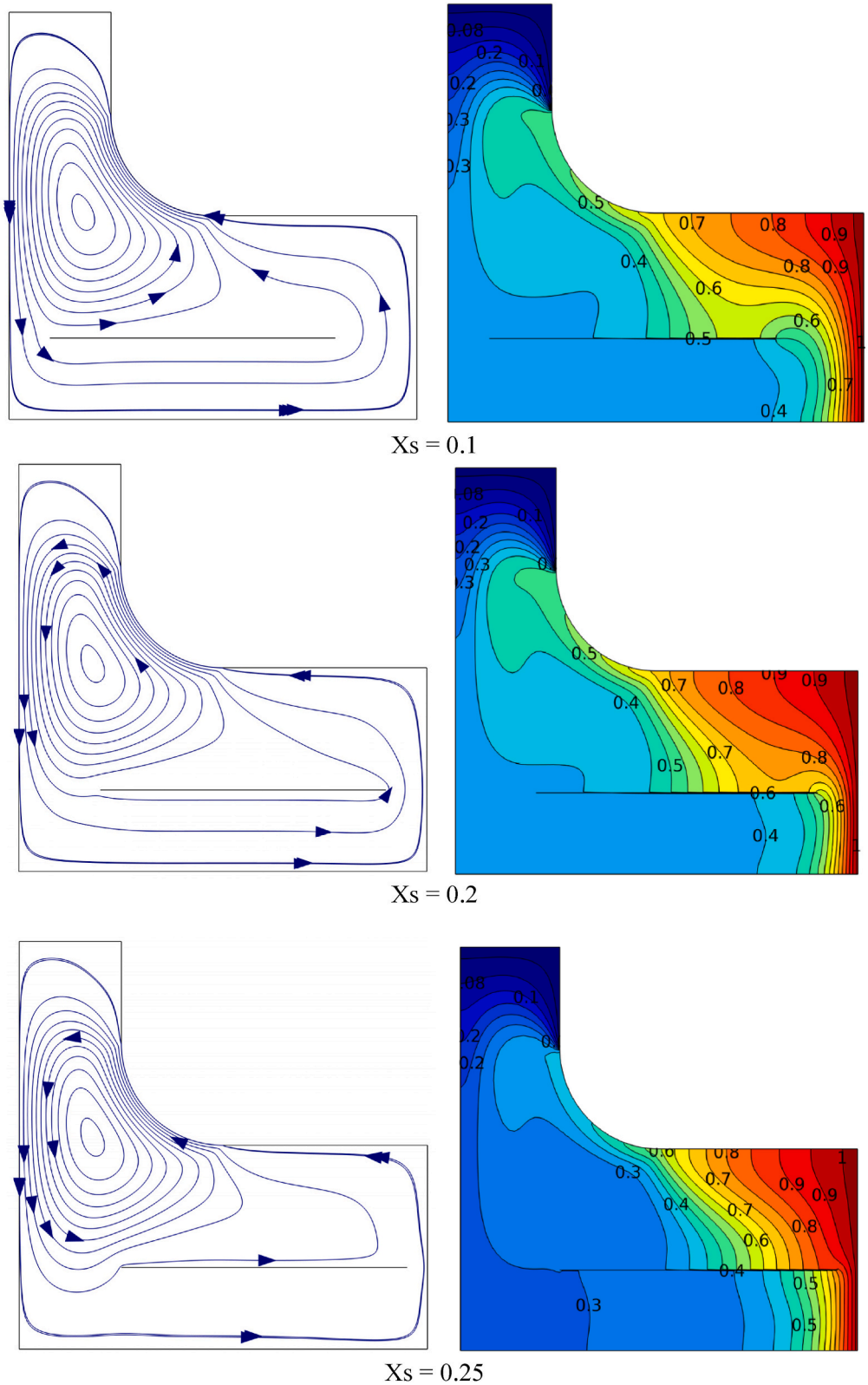

Fig. 16. Impact of the splitter horizontal position Xs, on the isotherms and the streamlines for Re = 200, Rad = 2, Ys = 0.2.

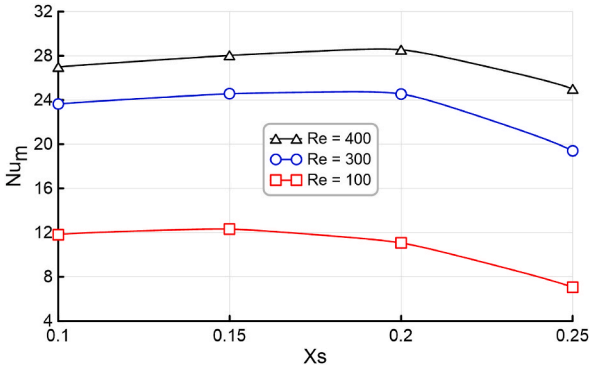

Fig. 17. Mean Nusselt number with the splitter horizontal position Xs and different Re numbers.

Consequently, it is wise to seek for the optimized position of the splitter.

4.6. The optimized position of the splitter

As it was observed how the splitter position affects the structure of streaming fluid and the temperature distribution, it become necessary to estimate its optimum position that gives maximal Nu_m. As it ascertained that Nu_m is a proportional functions to the radiation parameter and the Reynolds number, thus, these two parameters are not included as optimization parameter. Instead, we focused on the horizontal and vertical distances, Xs and Ys. The objective function is set as Max. (Nu_m), and the optimization iteration are performed for Rad = 3 and for different Re's numbers. The results are shown in Fig. 18 for Re = 100, 300 and 500. The optimized parameters are the horizontal (Xs = 0.05 – 0.25) and vertical (Ys = 0.1 – 0.45) positions of the splitter. These ranges are limited by the space of the cavity. Precisely, the optimum position for each Reynolds number is given Table 4. The optimization data show that with higher Reynolds number, the maximum Nu_m is obtained by displacing the splitter from the rotating ASS and from the symmetric line of the computational domain.

5. Conclusions

The current research focuses on the role of the rotating arc-shaped segment of a cavity wall and the inserted splitter in exciting the convection-radiation in a T-inverted cavity. Two rotating directions are explored and the position of the slitter is optimized using the Nelder-Mead method. The numerical discretization implemented in this research is validated with experimental study. The conclusions are summarized as follow.

1. Rotating the cylinder (arc-shaped segment) in clockwise direction produces streaming circulation consonant with buoyancy force, making this direction superior than the counterclockwise rotation, which produces counter rotating vortices, resisting the buoyancy force.
2. The splitter suggests an efficient tool in improving the convective-radiative heat removing, where about 19% increase can be attained at Re = 200.
3. Displacing the splitter closer to the rotating are-shape segment results in blocking the main vortex and repel the strength of streamlines passing towards the hot wall.
4. The algorithm of Nelder-Mead optimization has predicted the optimum position of the splitter for a given Re number. The optimization results suggest that with elevating the Reynolds number, the position of the splitter should be displaced from the symmetric lines of the solution domain and from the arc-shape rotating segment.
5. The radiation parameter and the Reynolds number escalate the mean Nusselt number due to enhanced inertial forces. Considering Rad = 0 as a reference case, the Nusselt number for Rad = 3 and 5 at Re = 300 increases by 197% and 282%, respectively. Additionally, leveraging Re from 200 to 500, the rise in the Nusselt number is 53%, 67%, and 79% for Rad = 0, 3, and 5, respectively.

CRediT authorship contribution statement

Muneer Ismael: Writing – review & editing, Writing – original draft, Methodology, Formal analysis. **Mohamed Bechir Ben Hamida:** Writing – review & editing, Writing – original draft, Validation, Software, Methodology, Formal analysis, Conceptualization. **Mehdi Ghalambaz:** Writing – review & editing, Writing – original draft, Methodology, Formal analysis, Conceptualization.

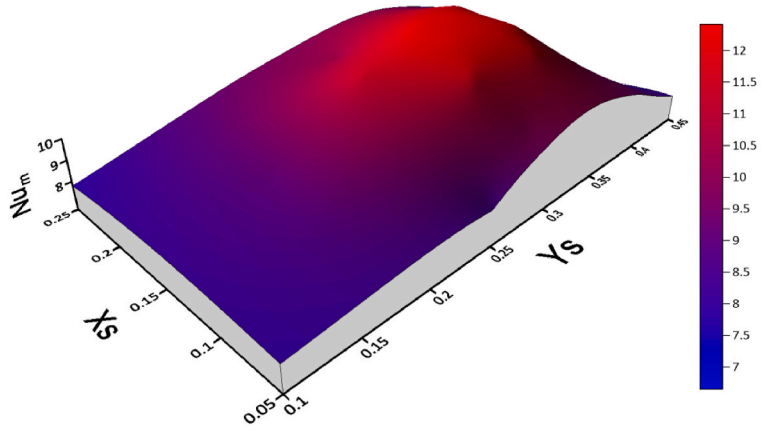

(A) Re = 100

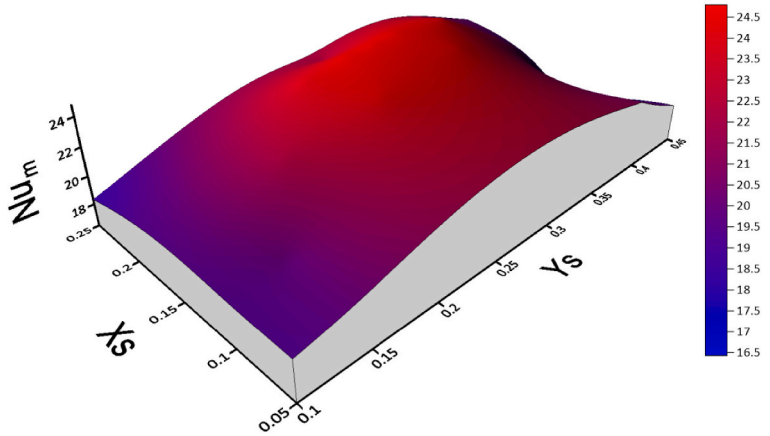

(B) Re = 300

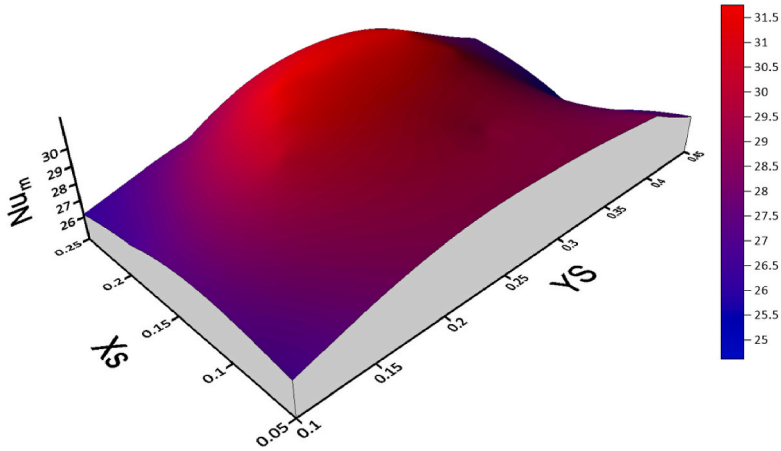

(C) Re = 500

Fig. 18. Optimized splitter location, Xs and Ys for three Reynolds numbers.

Table 4
The optimized locations of the splitter for different Re's number and Rad = 3.

Re	Optimized position		Max. (Nu_m)
	Xs	Ys	
100	0.1444	0.3213	12.417
200	0.1610	0.3049	19.695
300	0.1760	0.2814	24.793
400	0.1899	0.2765	28.639
500	0.2020	0.2617	31.753

Limitations and future work

This study is limited to laminar flow and Newtonian fluids. Future work should consider higher Reynolds numbers and non-Newtonian fluids. Additionally, the counterclockwise rotation of the ASS presents numerical instability issues, which warrant further investigation.

Funding statement

This work was supported and funded by the Deanship of Scientific Research at Imam Mohammad Ibn Saud Islamic University (IMSIU) (grant number IMSIU-DDRSP-RP26).

Declaration of competing interest

The authors declare no competing interests.

Data availability

Data will be made available on request.

References

[1] Tae Soo Choi, Eung Soo Kim, Numerical investigation of turbulent lid-driven flow using weakly compressible smoothed particle hydrodynamics CFD code with standard and dynamic LES models, Nucl. Eng. Technol. 55 (9) (2023) 3367–3382.
[2] M. Hadavand, S. Yousefzadeh, O.A. Akbari, F. Pourfattah, H.M. Nguyen, A. Asadi, A numerical investigation on the effects of mixed convection of Ag-water nanofluid inside a sim-circular lid-driven cavity on the temperature of an electronic silicon chip, Appl. Therm. Eng. 162 (2019) 114298.
[3] R. Iwatsu, J.M. Hyun, K. Kuwahara, Mixed convection in a driven cavity with a stable vertical temperature gradient, Int. J. Heat Mass Tran. 36 (6) (1993) 1601–1608.
[4] M.R. Sharif, Laminar mixed convection in shallow inclined driven cavities with hot moving lid on top and cooled from bottom, Appl. Therm. Eng. 27 (5-6) (2007) 1036–1042.
[5] K. Yapici, S. Obut, Benchmark results for natural and mixed convection heat transfer in a cavity, Int. J. Numer. Methods Heat Fluid Flow 25 (5) (2015) 998–1029.
[6] M.A. Alomari, K. Al-Farhany, Q.H. Al-Salami, K. Al-Jaburi, F.Q. Alyousuf, I.R. Ali, N. Biswas, Magnetohydrodynamic mixed convection in lid-driven curvilinear enclosure with nanofluid and partial porous layer, J. Magn. Magn Mater. 582 (2023) 170952.
[7] A.K. Hussein, H. Togun, F.L. Rashid, A. Basem, A.M. Abed, M.A. Al-Obaidi, T. Abdulrazzaq, J.M. Dhabab, M.E.H. Attia, B. Ali, S.K. Rout, Mixed convection in trapezoidal enclosures containing mono and hybrid nanofluids: a comprehensive review, J. Braz. Soc. Mech. Sci. Eng. 47 (4) (2025) 176.
[8] G.R. Kefayati, Double-diffusive mixed convection of pseudoplastic fluids in a two sided lid-driven cavity using FDLBM, J. Taiwan Inst. Chem. Eng. 45 (5) (2014) 2122–2139.
[9] A.K. Nayak, A. Haque, A. Banerjee, Thermosolutal mixed convection of a shear thinning fluid due to partially active mixed zones within a lid-driven cavity, Int. J. Heat Mass Tran. 106 (2017) 686–707.
[10] M.A. Alomari, K. Al-Farhany, A. Alajmi, A.M. Sadeq, N. Biswas, F. Alqurashi, M.A. Flayyih, Numerical modeling of MHD double-diffusive convection and entropy generation in an inclined curvilinear lid-driven cavity, Energy Sci. Eng. 13 (5) (2025) 2297–2314.
[11] A.S. Abedallh, O.R. Alomar, N.J. Yasin, Numerical and experimental investigation on mixed convection heat transfer inside cavity heated from below with reciprocating moving upper surface, Int. Commun. Heat Mass Tran. 159 (2024) 108242.
[12] K.B. Saleem, M.A. Ismael, A. Eladeb, B.M. Alshammari, L. Kolsi, The combined effect of mixed convective flow and CNT on the phase change process in an enclosure equipped with an oscillating heated base, Alex. Eng. J. 129 (2025) 911–924.
[13] M.A. Alomari, K. Al-Farhany, Q.H. Al-Salami, I.R. Ali, N. Biswas, M.H. Mohamed, F. Alqurashi, Numerical analysis to investigate the effect of a porous block on MHD mixed convection in a split lid-driven cavity with nanofluid, Int. J. Thermofluids 22 (2024) 100621.
[14] M.A. Alomari, Q.H. Al-Salami, F.Q. Alyousuf, F. Alqurashi, M.A. Flayyih, Numerical analysis of magnetohydrodynamic mixed convection and entropy generation in a curvelinear lid-driven cavity with carbon nanotubes and an adiabatic cylinder, Int. J. Thermofluids 24 (2024) 100852.
[15] C.H. Blohm, H.C. Kuhlmann, The two-sided lid-driven cavity: experiments on stationary and time-dependent flows, J. Fluid Mech. 450 (2002) 67–95.
[16] A.J. Chamkha, M.A. Ismael, Magnetic field effect on mixed convection in lid-driven trapezoidal cavities filled with a Cu–water nanofluid with an aiding or opposing side wall, J. Therm. Sci. Eng. Appl. 8 (3) (2016) 031009.
[17] M.A. Ismael, A.J. Chamkha, Mixed convection in lid-driven trapezoidal cavities with an aiding or opposing side wall, Numer. Heat Transf. A Appl. 68 (3) (2015) 312–335.
[18] S. Albensoeder, H.C. Kuhlmann, H.J. Rath, Multiplicity of steady two-dimensional flows in two-sided lid-driven cavities, Theor. Comput. Fluid Dynam. 14 (4) (2001) 223–241.
[19] M.A. Ismael, Numerical solution of mixed convection in a lid-driven cavity with arc-shaped moving wall, Eng. Comput. 34 (3) (2017) 869–891.
[20] M.A. Ismael, Double-diffusive mixed convection in a composite porous enclosure with arc-shaped moving wall: tortuosity effect, J. Porous Media 21 (4) (2018).

[21] H.K. Hamzah, F.H. Ali, M. Hatami, D. Jing, M.Y. Jabbar, Magnetic nanofluid behavior including an immersed rotating conductive cylinder: finite element analysis, Sci. Rep. 11 (1) (2021) 4463.
[22] M.Y. Jabbar, H.K. Hamzah, F.H. Ali, S.Y. Ahmed, M.A. Ismael, Thermal analysis of nanofluid saturated in inclined porous cavity cooled by rotating active cylinder subjected to convective condition, J. Therm. Anal. Calorimetry 144 (4) (2021) 1299–1323.
[23] Y. Ma, R. Mohebbi, M.M. Rashidi, Z. Yang, Mixed convection characteristics in a baffled U-shaped lid-driven cavity in the presence of magnetic field, J. Therm. Anal. Calorimetry 140 (4) (2020) 1967–1984.
[24] F.M. Azizul, A.I. Alsabery, I. Hashim, R. Roslan, H. Saleh, MHD mixed convection and heatlines approach of nanofluids in rectangular wavy enclosures with multiple solid fins, Sci. Rep. 13 (1) (2023) 9660.
[25] E.M. Hemmat, A.A.A. Abbasian, W.M. Yan, A. Aghaie, M. Afrand, N. Sina, Mixed convection of functionalized DWCNT-water nanofluid in baffled lid-driven cavities, Therm. Sci. 22 (6 Part A) (2018) 2503–2514.
[26] Y.Y. Ji, D.K. Sohn, H.S. Ko, The effect of baffles on vertical wall PCM to enhance natural convection, Int. J. Heat Mass Tran. 222 (2024) 125187.
[27] G. Lorenzini, B.S. Machado, L.A. Isoldi, E.D. Dos Santos, L.A.O. Rocha, Constructal design of rectangular fin intruded into mixed convective lid-driven cavity flows, J. Heat Tran. 138 (10) (2016) 102501.
[28] H. Moayedi, N. Amanifard, H.M. Deylami, A comparative study of the effect of fin shape on mixed convection heat transfer in a lid-driven square cavity, J. Braz. Soc. Mech. Sci. Eng. 44 (8) (2022) 322.
[29] M.M. Ali, R. Akhter, M.A. Alim, Magneto-mixed convection in a lid driven partially heated cavity equipped with nanofluid and rotating flat plate, Alex. Eng. J. 61 (1) (2022) 257–278.
[30] R. Akhter, M.M. Ali, M.A. Alim, Magnetic field impact on double diffusive mixed convective hybrid-nanofluid flow and irreversibility in porous cavity with vertical wavy walls and rotating solid cylinder, Results Eng. 19 (2023) 101292.
[31] R. Akhter, M.M. Ali, M.M. Billah, M.N. Uddin, Hybrid-nanofluid mixed convection in square cavity subjected to oriented magnetic field and multiple rotating rough cylinders, Results Eng. 18 (2023) 101100.
[32] M.M. Ikram, G. Saha, S.C. Saha, Conjugate forced convection transient flow and heat transfer analysis in a hexagonal, partitioned, air filled cavity with dynamic modulator, Int. J. Heat Mass Tran. 167 (2021) 120786.
[33] M.M. Ikram, G. Saha, S.C. Saha, Second law analysis of a transient hexagonal cavity with a rotating modulator, Int. J. Heat Mass Tran. 221 (2024) 125039.
[34] M.M. Ikram, G. Saha, S.C. Saha, Unsteady conjugate heat transfer characteristics in hexagonal cavity equipped with a multi-blade dynamic modulator, Int. J. Heat Mass Tran. 200 (2023) 123527.
[35] E.V. Shulepova, M.A. Sheremet, H.F. Oztop, N. Abu-Hamdeh, Mixed convection–radiation in lid-driven cavities with nanofluids and time-dependent heat-generating body, J. Therm. Anal. Calorimetry 146 (2) (2021) 725–738.
[36] K. Mehmood, S. Hussain, M. Sagheer, Numerical simulation of MHD mixed convection in alumina–water nanofluid filled square porous cavity using KKL model: effects of non-linear thermal radiation and inclined magnetic field, J. Mol. Liq. 238 (2017) 485–498.
[37] T. Basak, S. Roy, T. Paul, I. Pop, Natural convection in a square cavity filled with a porous medium: effects of various thermal boundary conditions, Int. J. Heat Mass Tran. 49 (7-8) (2006) 1430–1441.
[38] J.A. Nelder, R. Mead, A simplex method for function minimization, Computer J. 7 (4) (1965) 308–313.